scientific reports

Check for updates

OPEN

Identification of driving behavior in continuous diverging sections of expressway system interchange based on CNN-BiLSTM

Guanghui Sun[1], Hongbin Zhang[1]✉, Liande Zhong[2] & Qingqing Li[1]

The driving environment in continuous diverging sections of expressway system interchanges is highly complex, posing significant driving risks. To investigate driving behavior and its transition patterns in these areas, a simulated driving experiment was conducted to collect driving behavior parameters and construct a driving behavior spectrum (DBS) for continuous diverging sections. A driving behavior spectrum unit decomposition model, leveraging convolutional neural networks (CNN) and bidirectional long short-term memory networks (BiLSTM), was developed to identify specific driving behaviors. Additionally, a Hidden Markov Model (HMM) was employed to quantify transitions between various driving behavior states. The findings demonstrate that the DBS effectively captures and systematically records temporal changes in driving behavior. The CNN-BiLSTM model accurately identified four typical driving behaviors—straight driving, lane changing, deceleration, and turning—with an impressive average accuracy of 98%. Analysis revealed that the first lane change typically occurs approximately 121 m before the first diverging point, while the second occurs around 78 m before the second diverging point. Furthermore, the HMM model successfully elucidated the transition patterns between different driving states. These results provide valuable insights for identifying hazardous zones and optimizing facility design in expressway system interchanges.

Keywords Expressway, Diverging section, Driving behavior spectrum, CNN-BiLSTM, Hidden Markov model

In China, the total length of expressways has been steadily increasing, surpassing 180,000 km by the end of 2023. Interchanges play a pivotal role in the functionality of expressway systems and are generally classified into two categories: service interchanges and system interchanges. System interchanges, as grade-separated junctions, are specifically designed to enable seamless and efficient traffic transitions between expressways. However, this specialized function poses significant challenges for drivers. In system interchange areas, particularly within continuous diverging zones, drivers are required to perform multiple tasks, such as executing lane changes and adjusting speed, often within a short time frame. These rapid and dynamic transitions in driving behavior significantly elevate driving risks[1,2]. Consequently, accurately identifying distinct driving behaviors in the continuous diverging zones of expressway system interchanges and quantifying the transition patterns between these behaviors are critical for improving expressway traffic safety.

In the field of driving behavior analysis and expressway interchange safety, extensive research has been conducted to investigate driving behavior characteristics in various scenarios, particularly in high-risk environments such as ramps and merge/diverge areas of interchanges[3]. A large number of studies have employed driving simulator data or unmanned aerial vehicle (UAV) data for lane-changing intention prediction, providing valuable insights into driving behavior[4]. For example, Gu et al.[5] utilized UAVs to collect vehicle operation data in expressway merging areas and proposed a multi-level random parameter logistic regression model to analyze drivers' merging behavior on acceleration lanes and the factors influencing it. UAVs, with their high resolution and wide coverage, have been extensively used for traffic flow monitoring and driving intention prediction in expressway merging zones. Although the application of UAVs in traffic research is still in its early stages, their mobility and flexibility offer significant potential for future safety diagnostics and incident detection. However, UAV data is primarily limited to the macroscopic aspects of vehicle movement, making it difficult to obtain

[1]School of Transportation and Vehicle Engineering, Shandong University of Technology, Zibo 255000, China. [2]Research Institute of Highway Ministry of Transport, Beijing 100089, China. ✉email: hongbin_1979@163.com

microscopic data such as vehicle control operations, changes in driver behavior (e.g., steering, throttle, and braking), or driver physiological indicators.

In comparison, driving simulators can effectively address these limitations. By constructing specific scenarios, driving simulation experiments can not only collect macroscopic vehicle motion data but also simultaneously capture vehicle control data and drivers' psychological and physiological indicators. For example, Liu et al.[6] used driving simulation experiments to collect detailed driving behavior data, analyzing the impact of optimized guide signs on driving behavior in expressway interchange areas, and evaluated the optimization effects using the non-integer rank RSR method. Similarly, Wang et al.[7] collected data on drivers' heart rates, vehicle speeds, and steering operations through driving simulation experiments, studying the associations between the characteristics of young drivers and their visual and physiological attributes at expressway exit ramps. Furthermore, Liu et al.[8] combined driving simulation, Building Information Modeling (BIM), and data mining techniques to analyze the effects of safety facilities in underground interchanges on driving safety and comfort. They proposed an analysis method based on acceleration disturbance and steering comfort loss values, providing valuable insights for optimizing the construction of underground interchanges and the design of traffic safety facilities.

Meanwhile, researchers have also developed various methods to analyze driving behavior characteristics and their influencing factors.For example, Guo et al.[9] explored the effects of geometric designs of speed-change lanes on driving behaviors by analyzing speed and acceleration characteristics in diverging and merging areas. Their findings, supported by driving simulation experiments, offer valuable insights into determining optimal speed-change lane lengths and evaluating the safety of such designs. Similarly, Li et al.[10] introduced the Collision Risk Index (CRI), a framework for evaluating driving risks in expressway entrance zones. By incorporating factors like speed variations and vehicle acceleration, the CRI model provides a quantitative basis for assessing risks in different traffic scenarios. Wu et al.[11] proposed the Driving Risk Surrogate (DRS) model, which integrates virtual energy properties with interaction risk perception based on potential field theory. Compared to traditional methods, the DRS model demonstrates superior performance in trajectory prediction and speed estimation, presenting a novel methodology for quantifying risks in complex traffic conditions.

As research advances, the concept of the driving behavior spectrum (DBS) has garnered increasing attention. DBS integrates data on drivers, vehicles, and the environment, providing a comprehensive framework for understanding driving behaviors and assessing associated risks. Recently, DBS has been utilized for classifying driving behaviors, identifying high-risk patterns, and analyzing driving characteristics under various road conditions. For example, Chen et al.[12] proposed the Driving Habit Graph (DHG), which models individual driving styles using nodes and arcs to represent driving behavior sequences. Experimental results demonstrated its potential for driving behavior modeling and the development of advanced driver-assistance systems. Wang et al.[13] employed graph-based construction methods to model aggressive driving behaviors, significantly enhancing risk prediction accuracy by incorporating time windows and driving characteristic variables.

Advanced machine learning models have also played a pivotal role in driving behavior recognition and risk assessment[14]. Liu et al.[15] introduced the SLAFusion method, which combines Symbolic Aggregate Approximation (SAX) with Long Short-Term Memory (LSTM) networks to improve the detection of hazardous driving behaviors. This method excels in multi-granularity driving process modeling and feature fusion, achieving superior performance. Song et al.[16] applied a Random Forest classifier to develop a driver risk evaluation model, effectively classifying risk levels based on driving behavior characteristics and providing a reliable tool for early identification of high-risk drivers. Chen et al.[17] developed a transfer learning-based CNN model to identify unfavorable driving states using EEG signals and functional connectivity graphs, achieving 90% recognition accuracy. This highlights the potential of machine learning in driving behavior analysis.

While prior research has extensively addressed safety analyses of expressway interchanges, the construction of driving behavior spectrums, and the classification of driving behaviors, limited attention has been given to the recognition of driving behaviors and the transition patterns between different states in complex scenarios such as continuous diverging zones in expressway system interchanges. This study aims to bridge this gap by conducting a simulated driving experiment to construct a driving behavior spectrum for continuous diverging sections. A decomposition model of driving behavior spectrum units is developed using a convolutional neural network (CNN) combined with a bidirectional long short-term memory (BiLSTM) network to recognize different driving behaviors. Additionally, a Hidden Markov Model (HMM) is employed to quantitatively analyze the transition processes between various driving behaviors.

Methods

Data collection

The mainstream methods for data collection in driving behavior research are real vehicle experiments and driving simulation experiments. Real vehicle experiments face challenges in controlling environmental and external variables, resulting in lower safety and substantial influence from traffic flow. In contrast, driving simulation experiments replicate real driving conditions within a virtual environment, making them particularly suitable for studying high-risk scenarios or those that are difficult to observe in real-world settings. This study employs driving simulation experiments to gather data due to their controlled environment and flexibility. To ensure the reliability and validity of the simulation-derived data, real vehicle experiment data are also integrated for cross-validation. This combined approach enhances the robustness of the findings and ensures their applicability to real-world driving scenarios.

Virtual environment setup and experimental equipment

The virtual environment and experimental equipment used in this study are shown in Fig. 1. Figure 1a illustrates the design of the continuous diverging exit ramp at the Zibo West Interchange. The virtual environment was constructed using UC/Win-Road software to simulate the driving scenario. In this design, the expressway

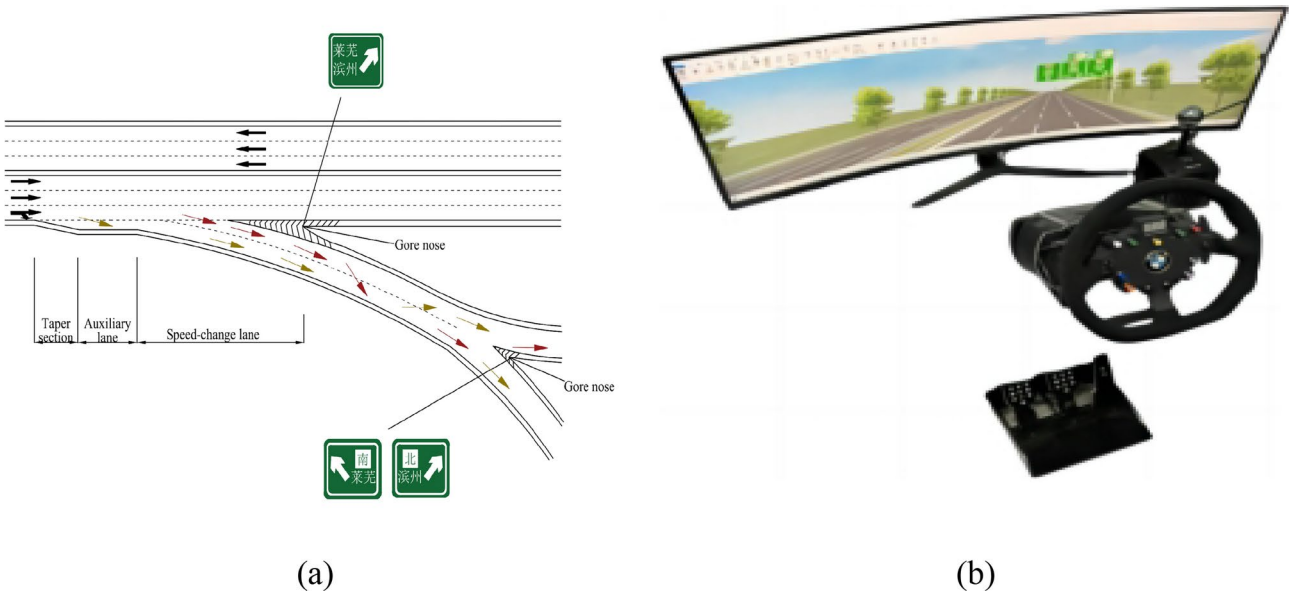

Fig. 1. Experimental Setup and Equipment (**a**) illustrates the schematic diagram of the experimental scene. (**b**) shows a 3D image of the equipment used in the experiment, derived from a real-world scene captured using a camera. Post-processing was conducted using Adobe Photoshop (version 24.1, https://www.adobe.com/photoshop), where surrounding background elements were removed to retain the core content.

mainline consists of six bidirectional lanes with a design speed of 120 km/h and a lane width of 3.75 m. The exit ramp adopts a dual-lane direct-type configuration, including a taper section of 90 m, a speed-change section of 225 m, and an auxiliary lane of 300 m. The exit taper rate is 1/22.5, and other traffic facilities are set according to the actual road conditions. Considering that vehicle speeds under free-flow conditions are generally higher than in other traffic states, which increases driving risks, this study focuses on driving conditions without traffic flow interference, where vehicles operate in free-flow conditions on the ramp.

The experimental equipment comprises a main computer, a wide-angle high-definition display, a steering wheel, accelerator and brake pedals, and a driver's seat, as illustrated in Fig. 1b, to replicate the driving environment as realistically as possible.

Participants

In the experimental process, the required sample size is estimated based on the expected variance, target confidence level, and margin of error. The calculation process is shown in Eq. (1):

$$N = \frac{\left(Z_{\alpha/2} + Z_{\beta}\right)^2 \cdot \sigma^2}{\varepsilon^2} \tag{1}$$

where $Z_{\alpha/2}$ represents the upper α/2 quantile of the standard normal distribution, which is typically associated with the confidence level. Z_{β} denotes the upper β quantile of the standard normal distribution, which is generally related to statistical power. σ represents the population standard deviation of the normal distribution, and ε is the margin of error, typically reflecting the difference between the mean of the response variable and the reference value.

A significance level of 10% is typically chosen to reflect a 90% confidence level for the unknown parameter. When the confidence level is 90%, $Z_{\alpha/2} = 1.65$. To balance validity and cost-effectiveness, an 80% statistical power is used, and when $\beta = 0.2$, $Z_{\beta} = 0.84$.While σ is often challenging to estimate, based on the relationship $\varepsilon = \pm d$, where d is the meaningful difference, the empirical range of σ is typically $0.25 \leq \sigma \leq 0.5$[18]. In this study, σ was set to 0.5. Accordingly, the minimum required sample size was calculated to be 25 participants. Additionally, in studies based on driving simulation technology related to road traffic safety and driver behavior, the number of participants generally ranges from 20 to 40[19–23]. Taking these considerations into account, the sample size for this study was set at 30 participants.

All participants were recruited from universities and the general public, including 18 males and 12 females, which aligns closely with the current demographic characteristics of drivers in China. The average age of the participants was 29 years, ranging from 23 to 41 years. All participants held valid C1 driver's licenses and had experience driving on expressway, with driving years ranging from 2 to 13 years. This study was approved by the Ethics Committee of Shandong University of Technology and was performed in accordance with the approved guidelines and the Declaration of Helsinki. All participants were informed about the study's content and objectives, and voluntarily participated in the experiment. And Informed consent was obtained from all subjects and/or their legal guardian(s).

Experimental procedure

The experiment consisted of four parts: (1) collection of participants' basic information, (2) training on the driving simulator, (3) a simulated driving test, and (4) the formal experiment. Before the formal experiment, all participants were required to register their basic information, including name, age, and driving experience. Although this information had already been collected during the recruitment process, a second verification was conducted before the participants proceeded to the training and experiment. Participants then underwent approximately 45 min of training, which included an introduction to the experimental scenarios and instructions on how to use the driving simulator. The purpose of the training was to familiarize participants with the experimental route and the operation of the simulator. Following the training, participants were allowed to practice on the driving simulator for as long as they wished, with no restrictions on time or the number of practice sessions, until they felt confident in operating the simulator. After completing the practice sessions, all participants were required to take a driving operation test. The test content and scores were automatically collected and generated by the driving simulator. Only participants who passed the test were permitted to proceed to the formal experiment.

In the formal experiment, participants were instructed to drive along the mainline at the designated speed. They first encountered a diverging section leading to a deceleration lane and then proceeded to a second diverging section before entering a ramp. Each participant experienced two diverging processes: the first diverging section (mainline diverging, where vehicles exit the expressway mainline) and the second diverging section (ramp diverging, where vehicles transition from the deceleration lane to their target ramp). After exiting the ramp, participants completed the experiment. The entire experiment was conducted in batches, with all participants divided into 5 groups, each consisting of six participants. One group was tested per day, and the total duration of the experiment was 5 days. In the morning, participants underwent training, practice, and testing, while the formal experiment was conducted in the afternoon. Participants took turns performing the experiment on the simulator. The experimental conditions were identical for all participants. After the experiment, the driving data from each participant were compiled and statistically analyzed.

Data preprocessing

In the formal experiment, the driving simulator automatically recorded the vehicle's speed, acceleration, throttle pedal input, and steering wheel rotation rate. To ensure the quality and reliability of the data, comprehensive data preprocessing was conducted after the experiment. The main goal of data preprocessing was to clean noisy data and standardize data formats, thereby providing high-quality data for subsequent analysis and modeling.

First, in terms of missing data handling, different strategies were adopted based on the proportion of missing values in the dataset. When the proportion of missing values was less than 5%, interpolation methods were used for imputation. If the proportion was higher, the corresponding data records were removed to minimize their impact on the analysis results.Second, for noise filtering, particularly high-frequency noise, we employed a low-pass filter as suggested by Campbell-Sills et al[24]. This technique was applied to smooth out high-frequency fluctuations in both driving behavior data (e.g., vehicle speed, steering wheel angle), rather than removing outliers. The low-pass filter allowed us to preserve important trends while minimizing noise.

Additionally, to eliminate the impact of different feature scales and enhance data comparability, numerical data (e.g., vehicle speed, steering wheel rotation rate,) were normalized. Generally, the Min–Max normalization method (as shown in Eq. 2) was used to linearly scale the data to the range [0,1]. However, for acceleration data, since its positive and negative signs only indicate the direction of acceleration or deceleration and do not directly reflect the magnitude of the value, bi-directional normalization (as shown in Eq. 3) was adopted. This method linearly scales the data to the range [− 1,1], preserving the directional characteristics of acceleration while ensuring that it remains comparable with other features within a unified range. This approach not only retains the directional information of acceleration but also ensures consistency with other features in the dataset.

$$x' = \frac{x - x_{\min}}{x_{\max} - x_{\min}} \tag{2}$$

$$x' = \frac{2(x - x_{\min})}{x_{\max} - x_{\min}} - 1 \tag{3}$$

where x represents the original data, x' represents the normalized data, x_{min} represents the minimum value in the dataset, and x_{max} represents the maximum value in the dataset.

Driving behavior spectrum construction and analysis

Construction of driving behavior spectrum

In practical applications, the Driving Behavior Spectrum (DBS) is a representation of a driver's psychological and physiological state, along with their control behaviors, mapped along the vehicle's travel direction at a specific moment. This concept captures multidimensional spatiotemporal driving data, as illustrated in Fig. 2. When the vehicle reaches a certain point, all driving behaviors exhibited by the driver at that moment—such as reactions, decisions, and control actions—constitute an element within the DBS. As the vehicle continues to travel, these elements accumulate, forming a sequential record of behaviors. From the vehicle's start to its stop, the aggregation of these elements constructs the complete DBS. This framework enables a comprehensive capture of a driver's behavioral characteristics over time, providing a richer and more detailed data foundation for driving behavior analysis and optimization. It facilitates a deeper understanding of driver actions and their evolution, offering valuable insights for improving driving safety and system design.

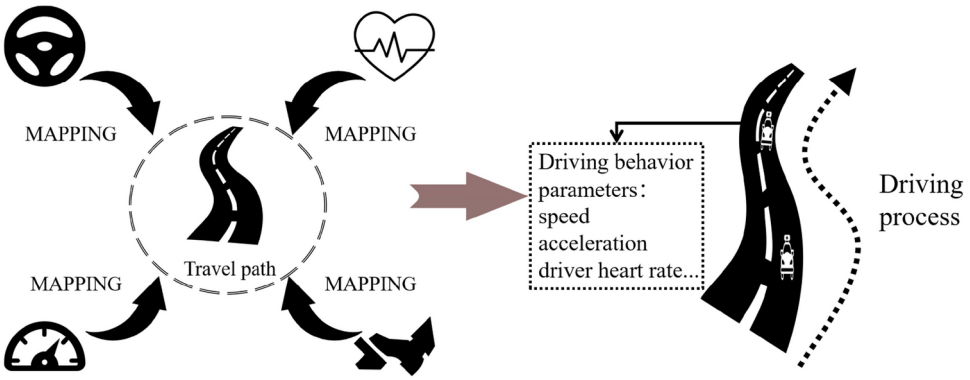

Fig. 2. Driving behavior spectrum.

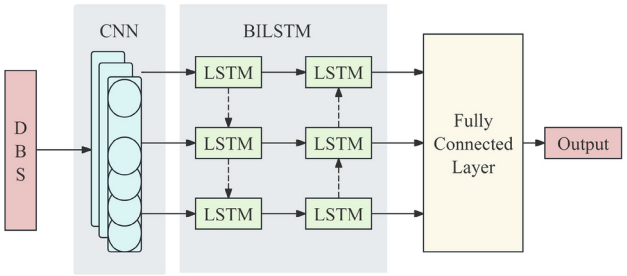

Fig. 3. CNN-BiLSTM model framework.

In a Driving Behavior Spectrum (DBS), multiple dimensions of driving behavior data are integrated, covering four key categories: the driver's data, vehicle operational status, road conditions, and environmental factors. The structure of the DBS is mathematically represented by Eq. 4:

$$I = [\ Dri_i \quad Veh_i \quad Roa_i \quad Eev_i\ ]^T \tag{4}$$

In this context, Dri_i represents the driver's information, Veh_i notes the vehicle's operational information, Roa_i refers to road conditions and Eev_i represents environmental factors. All these data collectively form the data matrix of the driving behavior spectrum, as shown in Eq. (5):

$$DBS = [I_1, I_2, I_3, \ldots, I_n] \tag{5}$$

In this study, the vehicle type is a passenger car, the road condition is the continuous diverging section of an expressway interchange, and the environmental condition is a clear morning.

Driving behavior spectrum decomposition method

The combination of Convolutional Neural Networks (CNN) and Bidirectional Long Short-Term Memory (BiLSTM) networks constitutes a powerful deep learning architecture commonly employed to process data with both spatial and temporal characteristics[25]. By integrating CNN's capability for local feature extraction with BiLSTM's sequential modeling strength, this approach effectively captures the intricate relationships and dynamic changes within driving behaviors[26]. CNN extracts local spatial features from driving data through convolutional layers, identifying correlations among different elements of the Driving Behavior Spectrum (DBS). At the same time, BiLSTM models temporal dependencies in driving behavior by processing time-series data in both forward and backward directions, thereby capturing the evolving patterns of driving behavior over time.

This combination leverages CNN's strength in extracting local features and BiLSTM's robust capacity for capturing temporal information, enabling the model to adapt effectively to variations in driving behaviors across different environments. Unlike traditional methods that depend on predefined rules or thresholds, this approach offers greater flexibility and adaptability[27].As a result, the CNN-BiLSTM architecture demonstrates notable advantages in both accuracy and applicability, making it suitable for diverse driving behavior spectrum data and varying operational conditions. The detailed model framework is illustrated in Fig. 3.

The CNN layer is designed to extract spatial features from the driving behavior spectrum data, which is implemented using two one-dimensional convolution layers (Conv1D). The driving behavior spectrum acts as the input to the model, as expressed in Eq. (6):

$$X = \begin{vmatrix} x_v^{(1)} & x_v^{(2)} & \cdots & x_v^{(k)} & \cdots & x_v^{(n)} \\ x_a^{(1)} & x_a^{(2)} & \cdots & x_a^{(k)} & \cdots & x_a^{(n)} \\ x_s^{(1)} & x_s^{(2)} & \cdots & x_s^{(k)} & \cdots & x_s^{(n)} \\ x_t^{(1)} & x_t^{(2)} & \cdots & x_t^{(k)} & \cdots & x_t^{(n)} \end{vmatrix} \tag{6}$$

In the equation, X represents the driving behavior spectrum, which includes five variables related to driving behavior: x_v is the speed, x_a is the acceleration, x_s is the steering wheel rotation rate, x_t is the throttle input value.

The first convolutional layer is designed to extract the local information of each feature. At this stage, the convolution operation processes each feature individually, without accounting for the relationships between adjacent time steps. The primary goal of this layer is to perform preliminary feature extraction at each specific time step. During the convolution operation, the ReLU (Rectified Linear Unit) activation function is applied. ReLU not only captures linear relationships within the data but also introduces non-linearity, enhancing the model's capacity to represent complex patterns and improving its overall performance in handling intricate problems. This process can be mathematically represented as shown in Eq. (7):

$$C = \mathrm{ReLU}(W \cdot X + b) \tag{7}$$

In the equation, X and C represent the input and output of the convolution, respectively; W is the weight matrix of the convolutional layer, b is the bias term.

The second convolutional layer is designed to extract local features of continuous behaviors within the time series. To avoid excessive reduction of important information during the convolution process, this layer is immediately followed by a max-pooling layer, which reduces the input feature dimensions by half. This operation preserves the most significant feature information, reduces computational complexity, improves model efficiency, and alleviates the risk of over fitting.

Through the combined convolution and pooling operations, the model effectively captures the local features within the driving behavior spectrum. These features serve as high-quality inputs for the BiLSTM network, thereby enhancing its capability to process and model time-dependent characteristics.

LSTM (Long Short-Term Memory) is a specialized variant of Recurrent Neural Network (RNN) designed to overcome the challenges of vanishing and exploding gradients often encountered in traditional RNNs. By addressing these issues, LSTM is particularly effective at capturing long-term dependencies in time-series data[28]. This is achieved through a sophisticated gating mechanism that regulates the flow of information and memory retention. This mechanism enables LSTM networks to maintain and utilize relevant information over extended sequences, making them highly effective for tasks involving complex temporal relationships[29].

An LSTM unit consists of three key gates, each responsible for different tasks related to information processing. Specifically, the Forget Gate decides which information should be discarded, filtering out irrelevant data. The Input Gate determines which new information will be stored in the unit's state, with new candidate values generated through the tanh activation function. The Output Gate controls which parts of the unit's state will contribute to the final output. The structure of the LSTM unit is shown in Fig. 4.

In Fig. 4, x_t represents the input at the current time step, and C_{t-1} is the memory cell state from the previous time step. The activation function sigmoid is used to regulate the flow of information in and out of the network. The Forget Gate updates the previous cell state C_{t-1}, the Input Gate determines which new information will be added to the state, and finally, the Output Gate decides the output at the current time step h_t. As indicated in Eq. (8), the weight matrices W_f、 W_t、 W_o and W_c correspond to the weights associated with the Forget Gate, Input Gate, Output Gate, and the state update, respectively, while b_f、 b_i、 b_c and b_o represent the biases for each gate. Through these operations, the previous cell state C_{t-1} is updated to the new cell state C_t and the output at the current time step h_t is generated.

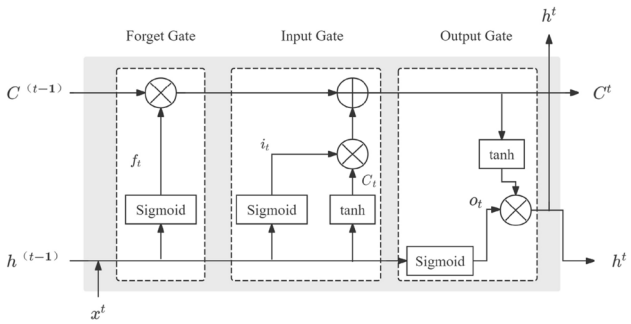

Fig. 4. LSTM network structure.

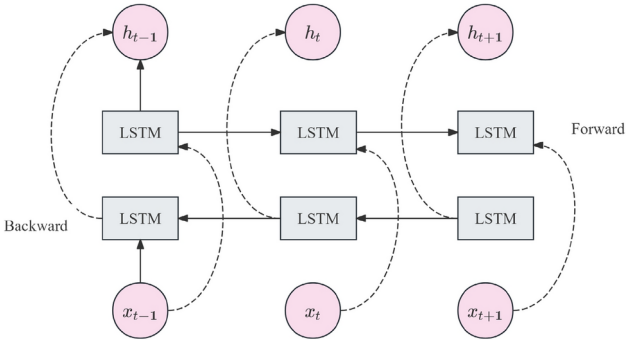

Fig. 5. BiLSTM structure.

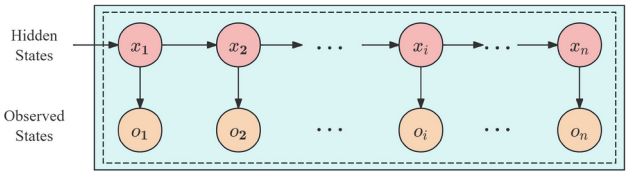

Fig. 6. Hidden Markov model (HMM) structure.

$$\begin{aligned} f_t &= \sigma(W_f \cdot [h_{t-1}, x_t] + b_f) \\ i_t &= \sigma(W_t \cdot [h_{t-1}, x_t] + b_i) \\ \widetilde{C}_t &= \tanh(W_c \cdot [h_{t-1}, x_t] + b_c) \\ o_t &= \sigma(W_o \cdot [h_{t-1}, x_t] + b_o) \end{aligned} \tag{8}$$

Bidirectional long short-term memory networks (BiLSTM) are an enhanced variant of traditional LSTM networks, designed to process input sequences in both forward and backward directions simultaneously[30]. Unlike standard LSTM, which captures temporal dependencies in only one direction, BiLSTM employs two independent LSTM networks: one processes the time series in the forward direction, while the other processes it in reverse[31]. This dual processing allows BiLSTM to capture richer global context information, making it particularly effective for tasks such as time series classification and recognition. The ability of BiLSTM to account for both preceding and succeeding time steps is especially valuable for time series data, where predictions at a given point often rely on patterns from both the past and future. BiLSTM is adept at capturing dynamic patterns, recognizing short-term variations while simultaneously uncovering long-term dependencies across multiple time periods. Moreover, time series data are frequently accompanied by noise and uncertainty. By integrating information from both directions, BiLSTM not only improves its ability to detect trends and respond to sudden changes but also smooths the data, reducing the impact of noise. This enhances the model's stability and robustness. The structure of BiLSTM is shown in Fig. 5.

Transition between different driving behavior states

In the driving behavior spectrum, different driving behavior states exhibit Markov properties, meaning that the driving state at any given time depends solely on the previous state and is independent of earlier states. The Hidden Markov Model (HMM), an advanced probabilistic model derived from the Markov model, is widely used to describe the statistical characteristics of stochastic processes[32]. Unlike traditional Markov models, HMM introduces a hidden state chain, consisting of two stochastic processes: one governing the hidden state transitions and the other representing the observable output sequence. This dual-process framework allows HMM to effectively analyze complex systems with hidden dynamics. In the context of driving behavior analysis, HMM extends the capabilities of the Markov model by uncovering unobservable (hidden) driving behavior states. It offers a more precise description of the randomness and state transitions between different behaviors, making it a valuable tool for examining driving pattern changes. A classical HMM model consists of two core components:

Markov Chain: Describes the transition process between hidden states. Stochastic Process: Establishes the probabilistic relationship between hidden states and the observed sequence of values.

The structure of the HMM model is depicted in Fig. 6, illustrating how hidden states interact with observed driving behavior sequences, thereby highlighting the model's ability to reveal underlying patterns in stochastic processes.

The HMM consists of five core elements, denoted as $\lambda = (X, O, \pi, A, B)$, where X represents the set of hidden states, O represents the set of observed states, π represents the initial state distribution, A represents

the state transition probability matrix, and B represents the observation probability matrix. The set of hidden states represents the possible hidden states in the DBS, i.e., the latent driving behavior features. These states are typically unobservable, but they determine the generation of observed values. The set of observed states usually refers to the DBS in the time series, and these parameters can typically be directly observed. The initial state distribution describes the probability distribution of the DBS starting in each of the hidden states. The state transition probability matrix defines the probability of transition between each pair of hidden states, describing the variation patterns between different hidden states. The observation probability matrix defines the probability of each hidden state generating a particular observation value.

Overall process

(1) Establishing the DBS dataset for continuous diverging sections of expressway interchange areas: The dataset includes four types of time-series features: speed, acceleration, steering wheel rotation rate, throttle input value. All data are standardized. For the unlabeled data, the K-Means clustering algorithm is applied for preliminary classification, and the optimal number of clusters is determined using the Elbow Method, which generates the initial labels for the dataset. Subsequently, the dataset is randomly split into a training set and a testing set in an 8:2 ratio, ensuring balanced label distribution.

(2) Construction of the CNN-BiLSTM Model: First, the DBS data are fed into a 1D CNN layer with 64 filters and a kernel size of 1, followed by another 1D CNN layer with 64 filters and a kernel size of 3, to further extract feature correlations between vehicle states. The CNN layers primarily extract dynamic features of the vehicle. Then, a BiLSTM layer with 50 neurons is used for bidirectional processing of the sequential data, capturing the temporal features of vehicle states, with an additional LSTM layer further strengthening the sequential dependencies. To prevent overfitting, dropout is applied in both the BiLSTM and LSTM layers. Finally, a fully connected layer with 4 neurons is used to classify the driving behavior. The model is trained with a batch size of 100, Adam optimizer, cross-entropy loss function, and a learning rate of 0.001. To thoroughly assess model performance, accuracy (A), precision (P), recall (R), and F1 score are used as evaluation metrics[23]. The formulas for calculating these metrics are shown in Eq. (9).

$$\begin{aligned} A &= \frac{\mathrm{TP}+\mathrm{TN}}{\mathrm{TP}+\mathrm{FP}+\mathrm{FN}+\mathrm{TN}} \\ P &= \frac{\mathrm{TP}}{\mathrm{TP}+\mathrm{FP}} \\ R &= \frac{\mathrm{TP}}{\mathrm{TP}+\mathrm{FN}} \\ \mathrm{F1} &= \frac{2\mathrm{PR}}{\mathrm{P}+\mathrm{R}} \end{aligned} \tag{9}$$

In the equation, TP and FP represent true positives and false positives, respectively; FN and TN represent false negatives and true negatives, respectively.

(3) Build the Markov model. The latent driving behaviors identified by the CNN-BiLSTM model are used as hidden states, and the five fundamental parameters in the DBS are used as observable variables. In the simulated driving experiment, all participants start driving from the main expressway, so the initial state probability is set as $\pi = (1, 0, 0, 0)$. Based on this initial state, the other parameters of the HMM are solved to further determine the state transition rules of driving behavior.

Results

Running results of the CNN-BiLSTM model

Before applying the CNN-BiLSTM model for the identification and classification of driving behavior, the optimal number of clusters was determined to be K = 4 by using the elbow method (as shown in Fig. 7) in combination

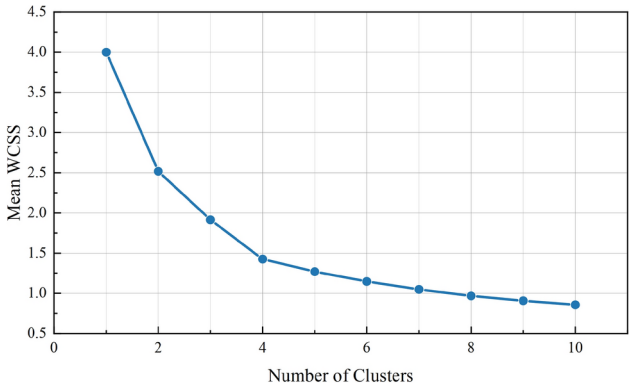

Fig. 7. Elbow method.

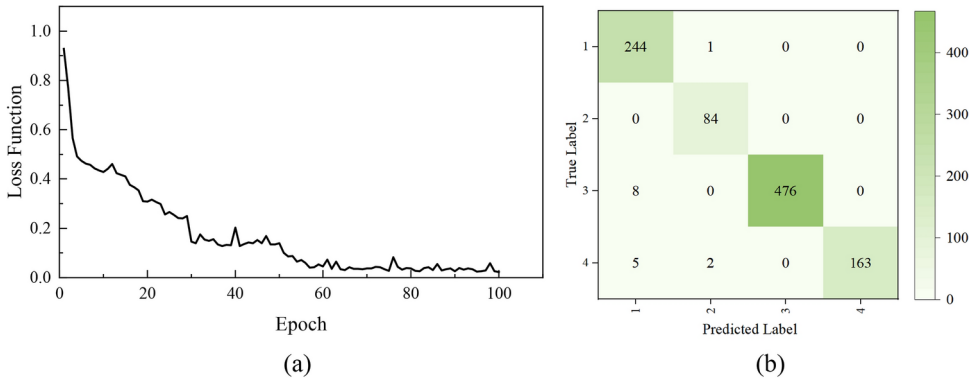

Fig. 8. Loss function curve and confusion matrix of the CNN-BiLSTM model.

Model Architecture	Accuracy	Precision	Recall	F1 Score
CNN-BiLSTM (Baseline)	0.98	0.98	0.98	0.98
BiLSTM Only	0.96	0.96	0.95	0.96
CNN Only	0.93	0.93	0.93	0.93
CNN-LSTM	0.95	0.95	0.95	0.95
BiLSTM without Regularization	0.94	0.94	0.94	0.94
CNN-BiLSTM with Sigmoid Activation	0.90	0.90	0.90	0.89

Table 1. Results of the ablation experiment.

with actual road alignment changes. The DBS data was then divided into four categories, which were used as the input for the CNN-BiLSTM model.

After 100 training epochs, the CNN-BiLSTM model achieved a final accuracy of 98% on the test set. The loss function trend, as shown in Fig. 8a, indicates a rapid decline in loss values during the initial training phase, stabilizing after approximately 60 epochs, which demonstrates good convergence performance. The model's confusion matrix, shown in Fig. 8b, further indicates high classification accuracy across the four categories of driving behaviors. To further verify the effectiveness of each module and its contribution to overall performance, an ablation study was designed and conducted. By progressively removing or replacing key components of the model, the impact of each module on the model's performance was analyzed, enabling a quantitative assessment of their roles in feature extraction, temporal modeling, and overall performance improvement. The experimental results, summarized in Table 1, show that the complete CNN-BiLSTM model outperforms other configurations, fully validating the collaborative advantage of CNN in local feature extraction and BiLSTM in global temporal modeling. When any module was removed, the model's performance declined significantly, indicating their indispensable roles in classification tasks. Additionally, the experiments revealed that bidirectional LSTMs outperformed unidirectional LSTMs in capturing complex temporal features, regularization techniques (such as Dropout) effectively reduced overfitting and improved the model's generalization ability, and ReLU activation functions demonstrated superior performance in nonlinear feature extraction compared to Sigmoid activation functions. These results further confirm that the structural design of the CNN-BiLSTM model is both reasonable and effective.

Identification results of different driving behaviors

The model classifies driving behavior in the DBS dataset into four distinct states, with the parameter distributions of each state shown in Fig. 9. The figure highlights significant differences in the distribution of five key features across the different driving states: State 1 represents high-speed straight driving, characterized by high speed (0.8–1.0), near-zero acceleration, high throttle input (0.8–1.0), low steering wheel rotation rate, typically occurring on straight road sections. State 2 corresponds to lane-changing, characterized by moderate speed (0.4–0.8), slightly positive acceleration, medium throttle input (0.4–0.8), and small directional adjustments. State 3 reflects deceleration driving, where both speed and throttle input are relatively low (0.3–0.6 and 0.2–0.6, respectively), acceleration with a distribution of negative values, and minimal steering adjustments are observed. State 4 represents turning, characterized by low speed (0.0–0.3), predominantly negative acceleration, low throttle input (0.0–0.4), a significant increase in steering wheel rotation rate. These observations indicate that driving behaviors in the continuous ramp diverging area can be categorized into four states: straight driving, lane-changing, deceleration, and turning.

The time-series mapping of different driving states is presented in Fig. 10. From the figure, it is evident that State 1 (high-speed straight driving) dominates from the start of the recorded data up to the 500-m exit sign,

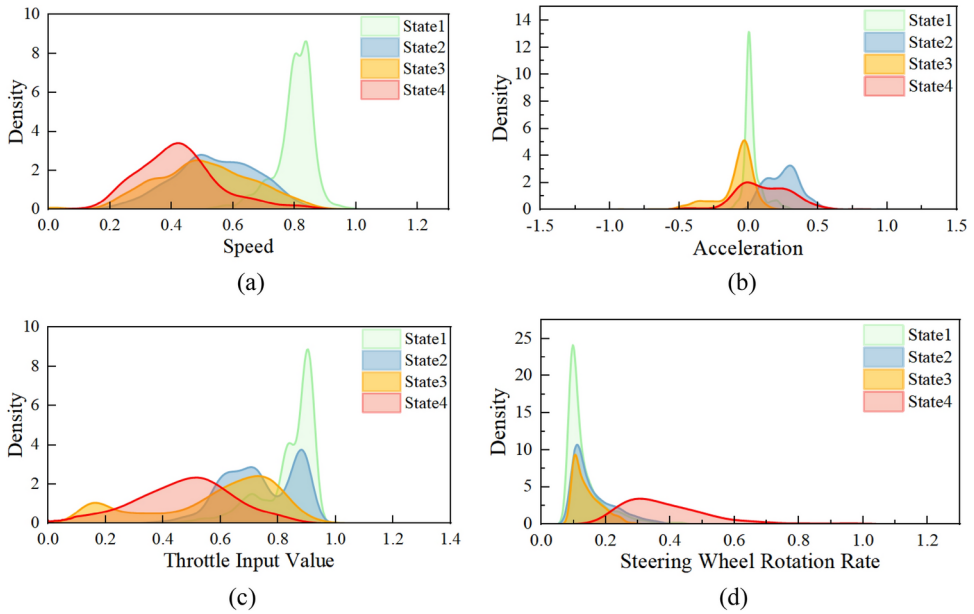

Fig. 9. Distribution differences of parameters for different states.

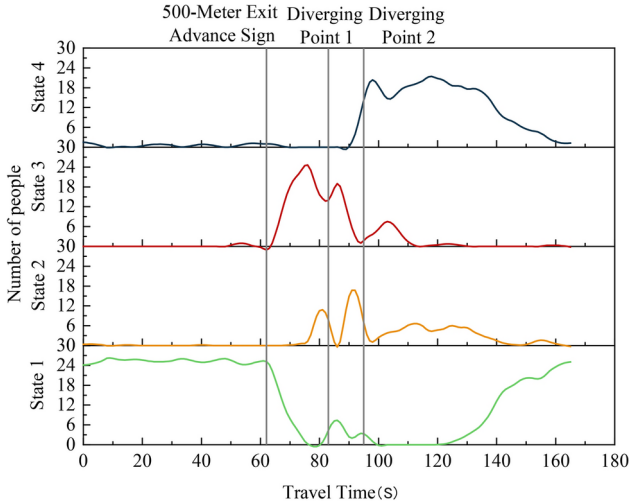

Fig. 10. Time mapping of different driving behavior states.

indicating that this segment primarily involves high-speed, straight-line driving. After passing the 500-m sign, the frequency of State 3 (deceleration driving) begins to increase, reflecting that drivers start slowing down in preparation for entering the diversion area. Approximately 10 s before reaching the first diverging point, the frequency of State 2 (lane-changing) rises sharply, indicating that vehicles begin changing lanes around 252 m before the diverging point. This activity peaks approximately 4 s before reaching the diverging point, or 121 m away, suggesting that most drivers complete their lane-changing maneuvers at this stage.

After passing the first diverging point, the frequency of State 3 (deceleration driving) rises again, indicating that vehicles have entered the ramp and are slowing down. Following this, the frequency of State 1 (high-speed straight driving) shows a slight increase, suggesting that some vehicles begin to accelerate. Approximately 12 s before the second diverging point (around 220 m before the point), the frequency of State 2 (lane-changing) begins to rise once more, indicating that some drivers, having determined their intended direction, proactively change to their target lane after entering the ramp. This activity peaks about 3 s before the second diverging point (around 78 m before the point), suggesting that most drivers complete the second lane-changing operation at this location. After passing the second diverging point, the frequency of State 4 (turning) reaches its peak, indicating that vehicles have completed the diversion and are now navigating the ramp in a turning maneuver.

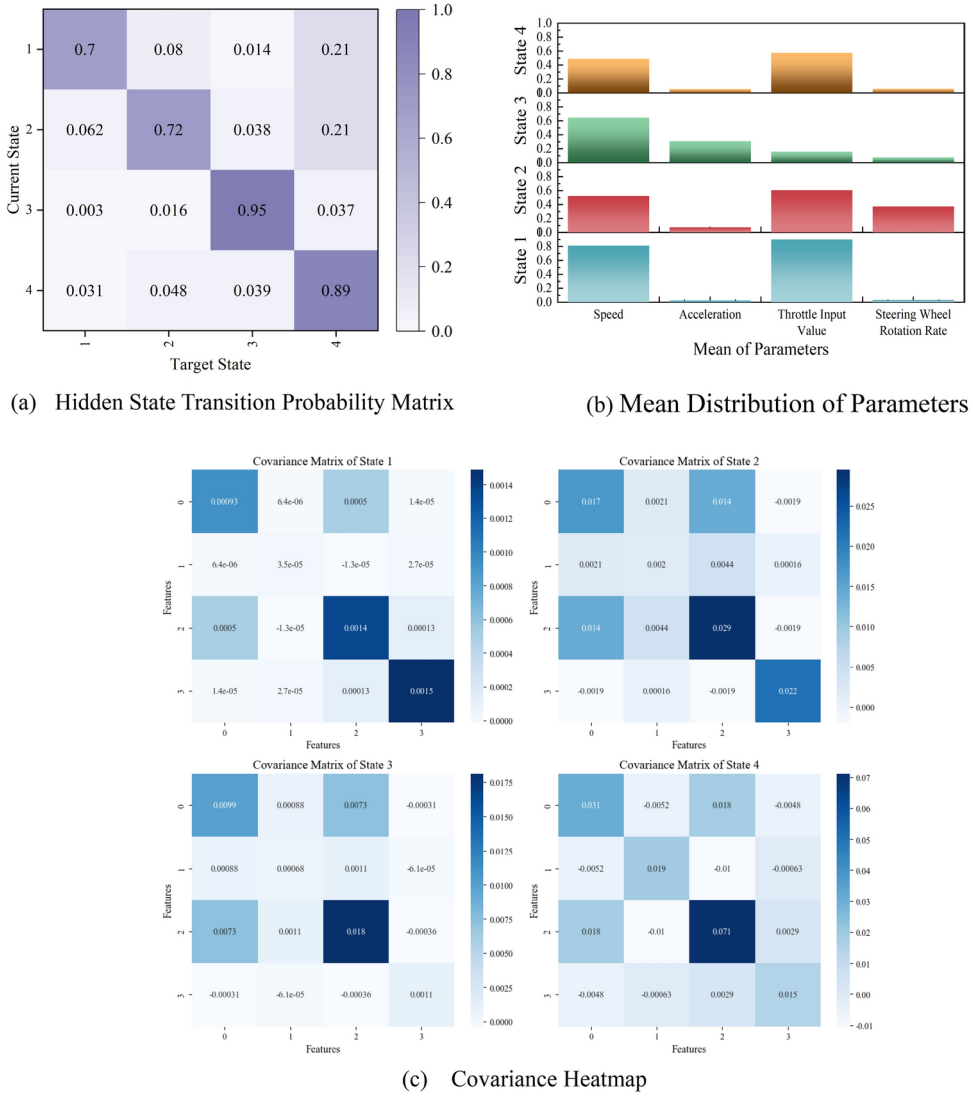

(a) Hidden State Transition Probability Matrix

(b) Mean Distribution of Parameters

(c) Covariance Heatmap

Fig. 11. Computation results of the hidden Markov model.

Analysis of transition between different driving behavior states

By solving the HMM model, the hidden state transition matrix is presented in Fig. 11a. The diagonal values are relatively high, indicating strong self-maintenance probabilities for the four distinct states. Specifically, the self-maintenance probability for state 1 is 0.7, while for state 4, it is 0.89. As the vehicle approaches the diverging point, the transition probabilities between states, particularly from the straight driving state to deceleration or lane-changing states, increase significantly. This observation is supported by the higher off-diagonal values in the transition matrix near the diverging point, reflecting the drivers' adaptive behaviors in response to changing environmental conditions.

The observation state probability matrix is described by a Gaussian distribution, which characterizes the distribution of observation values for each hidden state. The covariance matrix and mean distributions are shown in Fig. 11b, c, respectively. Figure 11b shows the mean features for each state. In the straight driving state, speed is high, acceleration is stable, and steering rate are low, indicating that the driver experiences a lighter load and focuses on maintaining speed. In deceleration or lane-changing states, the steering rate and acceleration fluctuate more, suggesting that the driver is more frequently adjusting and experiencing an increased number of driving tasks. These mean features indicate that the driver's load is lighter during straight driving, while more adjustments are required under complex driving conditions, demonstrating a higher level of adaptability. Figure 11c shows the covariance among the feature variables (features 0–3 represent speed, acceleration, throttle input, and steering wheel rotation rate). In the straight driving state, the covariance between speed and acceleration is low, indicating a weak linear relationship. This further suggests that the main road section is relatively smooth, with favorable traffic conditions, making the driving task less demanding. In the lane-changing state, the covariance between throttle input and steering wheel rotation rate is higher, reflecting the need for coordinated control. Notably, in the turning state, the covariance between speed, acceleration, and

steering wheel rotation rate increases, indicating a stronger interdependence among these variables. These covariance patterns emphasize how the driver's control behavior adapts to varying driving conditions.

Discussion

Multi-feature fusion in driving behavior spectrum analysis

This study constructs a comprehensive Driving Behavior Spectrum (DBS) by integrating multiple features such as speed, acceleration, throttle input Value, and steering wheel rotation rate .Many prior studies have focused on single-feature analysis, often considering only variations in speed or acceleration[33], which fail to capture the full spectrum of driving behavior. In contrast, this study utilizes multi-feature fusion to more accurately represent the variations in driver behavior across different scenarios, effectively reflecting their adaptability in complex traffic environments. Specifically, by analyzing the driving behavior spectrum, we obtain a more comprehensive understanding of driver states, particularly in complex traffic situations. For instance, in continuous diverging sections of expressway, drivers may adjust their behavior based on various factors, including speed, acceleration, and so on. This integrated approach to modeling behavior provides a solid foundation for the dynamic analysis of driving behaviors in complex road sections.

High-accuracy driving behavior recognition

As demonstrated in Fig. 8 and Table 1, the CNN-BiLSTM model achieved an impressive accuracy of 98.39% in driving behavior identification, significantly outperforming traditional methods[34,35]. Compared to rule-based or threshold-driven algorithms, CNN-BiLSTM is more adept at handling complex and rapidly changing driving behaviors, particularly in continuous diverging sections, where it can accurately capture shifts in driver behavior. Furthermore, the study found that drivers' lane-changing behavior at continuous diverging interchanges follows a certain pattern, which aligns with their proactive planning to change lanes as they approach diverging points, with the primary goal of avoiding conflicts with other vehicles. The study also revealed that the first lane change occurs approximately 121 m before the first diverging point, and the second lane change occurs 78 m before the second diverging point. Unlike the study by Chen et al.[36], this finding further refines the timing and positioning of lane changes. By identifying key lane-change positions, traffic management authorities can optimize lane divisions and road markings, thereby reducing the risk of traffic accidents.

Probability modeling of driving behavior transitions

This study further employs the Hidden Markov Model (HMM) to quantitatively analyze the transition probabilities between various driving behavior states. The quantitative analysis of state transitions through HMM allows for a clearer capture of the driver's adaptive behaviors at various stages, thereby providing deeper insights into their decision-making and behavioral adjustments as they approach diverging areas. Previous studies have shown that the probability of lane changing or deceleration increases significantly as drivers approach diverging points[37,38], though these transition probabilities have not been explicitly quantified. Notably, this study constructs a driving behavior transition probability model covering the entire process from the mainline to the taper section, Diverging Point 1, speed-change section, Diverging Point 2, and the target ramp (see Fig. 11), and quantifies the transition probabilities at each stage. This model holds significant reference value for the design of autonomous driving systems and route planning, particularly in the design of functional areas such as taper and speed-change sections.

Conclusion

This study presents a novel approach for analyzing driving behavior in continuous diverging sections of expressway interchanges using the Driving Behavior Spectrum (DBS), CNN-BiLSTM model, and Hidden Markov Model (HMM). By integrating multiple data sources, the framework effectively captures and quantifies driving behaviors and their transitions, achieving high accuracy in behavior recognition (98.33%). The study identifies key behaviors such as lane changing, deceleration, and turning, and reveals important patterns in driver adaptation near diverging points. The findings provide valuable insights for optimizing interchange design, enhancing traffic safety, and supporting the development of autonomous driving systems.

Data availability

The datasets generated and analyzed during the current study are available from the corresponding author on reasonable request.

Received: 22 November 2024; Accepted: 11 March 2025
Published online: 27 March 2025

References

1. He, H., Wang, B., Gao, Q. & Pang, X. How interchange spacing effects drivers' visual performance in high-density interchange groups—A naturalistic driving study. *Transp. Res. Part F Traffic Psychol. Behav.* **104**, 433–448. https://doi.org/10.1016/j.trf.2024.06.011 (2024).
2. Zeng, J., Wang, Y. & Chen, Z. Expressway traffic flow under the combined bottleneck of accident and on-ramp in framework of Kerner's three-phase traffic theory. *Physica A Stat. Mech. Appl.* **574**, 125918. https://doi.org/10.1016/j.physa.2021.125918 (2021).
3. Feknssa, N., Venkataraman, N., Shankar, V. & Ghebrab, T. Unobserved heterogeneity in ramp crashes due to alignment, interchange geometry and truck volume: Insights from a random parameter model. *Anal. Methods Accid. Res.* **37**, 100254. https://doi.org/10.1016/j.amar.2022.100254 (2023).
4. Outay, F., Mengash, H. A. & Adnan, M. Applications of unmanned aerial vehicle (UAV) in road safety, traffic and highway infrastructure management: Recent advances and challenges. *Transp. Res. Part A Policy Pract.* **141**, 116–129. https://doi.org/10.1016/j.tra.2020.09.018 (2020).

5. Gu, X., Abdel-Aty, M., Xiang, Q., Cai, Q. & Yuan, J. Utilizing UAV video data for in-depth analysis of drivers' crash risk at interchange merging areas. *Accid. Anal. Prev.* **123**, 159–169. https://doi.org/10.1016/j.aap.2018.11.010 (2019).
6. Liu, Q. et al. Study on optimization design of guide signs in dense interchange sections of eight-lane freeway. *Accid. Anal. Prev.* **209**, 107828. https://doi.org/10.1016/j.aap.2024.107828 (2025).
7. Wang, Z. et al. Correlation analysis between young driver characteristics and visual/physiological attributes at expressway exit ramp. *Engineering* **5**, 1435–1450. https://doi.org/10.3390/eng5030076 (2024).
8. Liu, Z., Yang, Q., Wang, A. & Gu, X. Vehicle driving safety of underground interchanges using a driving simulator and data mining analysis. *Infrastructures* **9**, 28. https://doi.org/10.3390/infrastructures9020028 (2024).
9. Guo, Z., Wan, H., Zhao, Y., Wang, H. & Li, Z. Driving simulation study on speed-change lanes of the multi-lane freeway interchange. *Procedia Soc. Behav. Sci.* **96**, 60–69. https://doi.org/10.1016/j.sbspro.2013.08.010 (2013).
10. Li, X., Wang, X. & Fu, X. Research on driving risk model of freeway interchange entrance area for accident prevention. *Procedia Soc. Behav. Sci.* **96**, 25–30. https://doi.org/10.1016/j.sbspro.2013.08.006 (2013).
11. Wu, R., Liu, H. & Zhang, Y. Integrated driving risk surrogate model and car-following behavior for freeway risk assessment. *Accid. Anal. Prev.* **201**, 107571. https://doi.org/10.1016/j.aap.2024.107571 (2024).
12. Chen, S., Fang, C. & Tien, C. Driving behaviour modelling system based on graph construction. *Transp. Res. Part C Emerg. Technol.* **26**, 314–330. https://doi.org/10.1016/j.trc.2012.10.004 (2013).
13. Wang, J., Feng, X., Zhang, Y. & Chen, L. Modeling aggressive driving behavior based on graph construction. *Transp. Res. Part C Emerg. Technol.* **138**, 103654. https://doi.org/10.1016/j.trc.2022.103654 (2022).
14. Valente, J., Ramalho, C., Vinha, P., Mora, C. & Jardim, S. Using machine learning to understand driving behavior patterns. *Procedia Comput. Sci.* **239**, 1823–1830. https://doi.org/10.1016/j.procs.2024.06.363 (2024).
15. Liu, J., Zhang, F. & Yang, H. SLAFusion: Attention fusion based on SAX and LSTM for dangerous driving behavior detection. *Inf. Sci.* **640**, 119063. https://doi.org/10.1016/j.ins.2023.119063 (2023).
16. Song, X., Liu, T. & Wang, Z. The mediating effect of driver characteristics on risky driving behaviors moderated by gender, and the classification model of driver's driving risk. *Accid. Anal. Prev.* **153**, 106038. https://doi.org/10.1016/j.aap.2021.106038 (2021).
17. Chen, J., Wang, H. & He, E. A transfer learning-based CNN deep learning model for unfavorable driving state recognition. *Cogn. Comput.* **16**, 121–130. https://doi.org/10.1007/s12559-023-10196-7 (2024).
18. Cochran, W. G. *Sampling Techniques* 3rd edn. (Wiley, 1991).
19. Vollrath, M., Schleicher, S. & Gelau, C. The influence of Cruise Control and Adaptive Cruise Control on driving behaviour—A driving simulator study. *Accid. Anal. Prev.* **43**, 1134–1139. https://doi.org/10.1016/j.aap.2010.12.023 (2011).
20. Duffney, R., Borowsky, A. & Bar-Gera, H. The effects of adaptive cruise control (ACC) headway time on young-experienced drivers' overtaking tendency in a driving simulator. *Transp. Res. Part F Traffic Psychol. Behav.* **86**, 151–160. https://doi.org/10.1016/j.trf.2022.02.008 (2022).
21. Alruwaili, A. & Xie, K. Modeling the influence of connected vehicles on driving behaviors and safety outcomes in highway crash scenarios across varied weather conditions: A multigroup structural equation modeling analysis using a driving simulator experiment. *Accid. Anal. Prev.* **199**, 107514. https://doi.org/10.1016/j.aap.2024.107514 (2024).
22. Zhao, X., Xu, W., Ma, J., Li, H. & Chen, Y. An analysis of the relationship between driver characteristics and driving safety using structural equation models. *Transp. Res. Part F Traffic Psychol. Behav.* **62**, 529–545. https://doi.org/10.1016/j.trf.2019.02.004 (2019).
23. Jing, D., Song, C., Guo, Z. & Li, R. Influence of the median opening length on driving behaviors in the crossover work zone: A driving simulation study. *Transp. Res. Part F Traffic Psychol. Behav.* **82**, 333–347. https://doi.org/10.1016/j.trf.2021.09.001 (2021).
24. Campbell-Sills, L., Barlow, D. H., Brown, T. A. & Hofmann, S. G. Effects of suppression and acceptance on emotional responses of individuals with anxiety and mood disorders. *Behav. Res. Ther.* **44**, 1251–1263. https://doi.org/10.1016/j.brat.2005.10.001 (2006).
25. Bai, X., Zhang, L., Feng, Y., Yan, H. & Quan, M. Multivariate temperature prediction model based on CNN-BiLSTM and RandomForest. *J. Supercomput.* **81**, 162. https://doi.org/10.1007/s11227-024-06689-3 (2025).
26. Ghimire, S., Deo, R. C., Casillas-Pérez, D. & Salcedo-Sanz, S. Efficient daily electricity demand prediction with hybrid deep-learning multi-algorithm approach. *Energy Convers. Manag.* **297**, 117707. https://doi.org/10.1016/j.enconman.2023.117707 (2023).
27. Luo, S., Wang, B., Gao, Q., Wang, Y. & Pang, X. Stacking integration algorithm based on CNN-BiLSTM-Attention with XGBoost for short-term electricity load forecasting. *Energy Rep.* **12**, 2676–2689. https://doi.org/10.1016/j.egyr.2024.08.078 (2024).
28. Ma, J., Liu, H., Peng, C. & Qiu, T. Unauthorized broadcasting identification: A deep LSTM recurrent learning approach. *IEEE Trans. Instrum. Meas.* **69**, 5981–6598. https://doi.org/10.1109/TIM.2020.3008988 (2020).
29. Zou, Z., Yan, X., Yuan, Y., You, Z. & Chen, L. Attention mechanism enhanced LSTM networks for latency prediction in deterministic MEC networks. *Intell. Syst. Appl.* **23**, 200425. https://doi.org/10.1016/j.iswa.2024.200425 (2024).
30. Ma, C., Hu, Y. & Xu, X. Hybrid deep learning model with VMD-BiLSTM-GRU networks for short-term traffic flow prediction. *Data Sci. Manag.* https://doi.org/10.1016/j.dsm.2024.10.004 (2024).
31. Li, Q., Cheng, R. & Ge, H. Short-term vehicle speed prediction based on BiLSTM-GRU model considering driver heterogeneity. *Physica A Stat. Mech. Appl.* **610**, 128410. https://doi.org/10.1016/j.physa.2022.128410 (2023).
32. Mauá, D. D., Antonucci, A. & de Campos, C. P. Hidden Markov models with set-valued parameters. *Neurocomputing* **180**, 94–107. https://doi.org/10.1016/j.neucom.2015.08.095 (2016).
33. Xu, J., Fu, J., Liu, X. & Shao, Y. Speed behavior of passenger cars on helical ramps and helical bridges in mountain riverside cities. *J. Adv. Transp.* **6**, 1–17. https://doi.org/10.1155/2018/6752574 (2018).
34. Ma, L., Qu, S., Song, L., Zhang, J. & Ren, J. Human-like car-following modeling based on online driving style recognition. *Electron. Res. Arch.* **31**, 3264–3290. https://doi.org/10.3934/era.2023165 (2023).
35. Zhu, S. et al. An optimized algorithm for dangerous driving behavior identification based on unbalanced data. *Electronics* **11**, 1557. https://doi.org/10.3390/electronics11101557 (2022).
36. Chen, S. et al. Analyzing differences in highway lane-changing behavior using vehicle trajectory data. *Physica A: Stat. Mech. Appl.* **624**, 128980. https://doi.org/10.1016/j.physa.2023.128980 (2023).
37. Karlsson, J., Murgovski, N. & Sjöberg, J. Optimal trajectory planning and decision-making in lane change maneuvers near a highway exit. In *2019 18th European Control Conference (ECC)*, 3254–3260 (IEEE, 2019).
38. Ma, Y., Zhang, W., Gu, X. & Zhao, J. Impacts of experimental advisory exit speed sign on traffic speeds for freeway exit ramps. *PLoS ONE* **14**, e0225203. https://doi.org/10.1371/journal.pone.0225203 (2019).

Author contributions

G.S.: Software, investigation, validation, formal analysis, visualization, writing—original draft. H.Z.: Conceptualization, methodology, validation, writing—review & editing, funding acquisition. L.Z.: Validation, resources. Q.L.: Visualization, writing—review & editing. All authors reviewed the manuscript.

Declarations

Competing interests
The authors declare no competing interests.

Additional information
Correspondence and requests for materials should be addressed to H.Z.

Reprints and permissions information is available at www.nature.com/reprints.

Publisher's note Springer Nature remains neutral with regard to jurisdictional claims in published maps and institutional affiliations.